Research Article | Vol. 24, No. 15 / 25 Jul 2016 / OPTICS EXPRESS 16366
Optics EXPRESS

Fabry-Pérot resonator: spectral line shapes, generic and related Airy distributions, linewidths, finesses, and performance at low or frequency-dependent reflectivity

NUR ISMAIL, CRISTINE CALIL KORES, DIMITRI GESKUS, AND MARKUS POLLNAU*

Department of Materials and Nano Physics, School of Information and Communication Technology, KTH – Royal Institute of Technology, Electrum 229, Isafjordsgatan 22–24, 16440 Kista, Sweden
**pollnau@kth.se*

Abstract: We systematically characterize the Fabry-Pérot resonator. We derive the generic Airy distribution of a Fabry-Pérot resonator, which equals the internal resonance enhancement factor, and show that all related Airy distributions are obtained by simple scaling factors. We analyze the textbook approaches to the Fabry-Pérot resonator and point out various misconceptions. We verify that the sum of the mode profiles of all longitudinal modes is the fundamental physical function that characterizes the Fabry-Pérot resonator and generates the Airy distribution. Consequently, the resonator losses are quantified by the linewidths of the underlying Lorentzian lines and not by the measured Airy linewidth. Therefore, we introduce the Lorentzian finesse which provides the spectral resolution of the Lorentzian lines, whereas the usually considered Airy finesse only quantifies the performance of the Fabry-Pérot resonator as a scanning spectrometer. We also point out that the concepts of linewidth and finesse of the Airy distribution of a Fabry-Pérot resonator break down at low reflectivity. Furthermore, we show that a Fabry-Pérot resonator has no cut-off resonance wavelength. Finally, we investigate the influence of frequency-dependent mirror reflectivities, allowing for the direct calculation of its deformed mode profiles.

OCIS codes: (230.5750) Resonators; (140.4780) Optical resonators; (140.3410) Laser resonators.

References and links

1. C. Fabry and A. Pérot, "Théorie et applications d'une nouvelle méthode de spectroscopie interférentielle," Ann. de Chim. et de Phys. **16**(7), 115–144 (1899).
2. J. M. Vaughan, *The Fabry-Pérot Interferometer* (Bristol and Philadelphia, 1989), Ch. 3.2.3., pp. 97–102.
3. J. M. Vaughan, *The Fabry-Pérot Interferometer* (Bristol and Philadelphia, 1989), Ch. 3.3.2., p. 105.
4. A. E. Siegman, *Lasers* (University Science Books, 1986), Ch. 11.4, pp. 428–430.
5. A. E. Siegman, *Lasers* (University Science Books, 1986), Ch. 11.3, pp. 413–428.
6. A. E. Siegman, *Lasers* (University Science Books, 1986), Ch. 11.5, pp. 432–440.
7. A. E. Siegman, *Lasers* (University Science Books, 1986), Ch. 11.1, pp. 398–408.
8. O. Svelto, *Principles of Lasers*, 5th ed. (Springer, 2010), Ch. 4.5.1, pp. 142–146.
9. O. Svelto, *Principles of Lasers*, 5th ed. (Springer, 2010), Ch. 5.3, pp. 169–171.
10. B. E. A. Saleh and M. C. Teich, *Fundamentals of Photonics*, 2nd ed. (Wiley-Interscience, 2007), pp. 571–572.
11. B. E. A. Saleh and M. C. Teich, *Fundamentals of Photonics*, 2nd ed. (Wiley-Interscience, 2007), Ch. 7.1B, pp. 254–257.
12. B. E. A. Saleh and M. C. Teich, *Fundamentals of Photonics*, 2nd ed. (Wiley-Interscience, 2007), Ch. 2.5B, pp. 62–66.
13. M. Eichhorn and M. Pollnau, "Spectroscopic foundations of lasers: Spontaneous emission into a resonator mode," IEEE J. Sel. Top. Quantum Electron. **21**(1), 486 (2015).
14. J. O. Stoner, "PEPSIOS purely interferometric high-resolution scanning spectrometer. III. Calculation of interferometer characteristics by a method of optical transients," J. Opt. Soc. Am. **56**(3), 370–376 (1966).
15. G. Koppelmann, "Multiple-beam interference and natural modes in open resonators," in *Progress in Optics*, Vol. 7, E. Wolf ed. (1969), Ch. 1, pp. 1–66.
16. F. Bayer-Helms, "Analyse von Linienprofilen. I Grundlagen und Messeinrichtungen," Z. Angew. Phys. **15**, 330–338 (1963).
17. J. B. Kumer and W. G. Uplinger, "Elsasser-related approximation to the Airy function," Appl. Opt. **22**(23), 3675–3676 (1983).

#261537 http://dx.doi.org/10.1364/OE.24.016366
Journal © 2016 Received 15 Apr 2016; revised 5 Jul 2016; accepted 6 Jul 2016; published 12 Jul 2016

Optics EXPRESS

18. J. M. Llorens, J. Buencuerpo, and P. A. Postigo, "Absorption features of the zero frequency mode in an ultra-thin slab," Appl. Phys. Lett. **105**(23), 231115 (2014).
19. J. W. Strutt, "Investigations in optics, with special reference to the spectroscope," Philos. Mag. **8**(49), 261–274, 403–411, 477–486 (1879).
20. I. Juvells, A. Carnicer, J. Ferré-Borrull, E. Martín-Badosa, and M. Montes-Usategui, "Understanding the concept of resolving power in the Fabry-Perot interferometer using a digital simulation," Eur. J. Phys. **27**(5), 1111–1119 (2006).
21. W. Kahan, "Further remarks on reducing truncation errors," Appl. Opt. **8**(1), 40 (1965).
22. R. Remmert, "Convergent series of meromorphic functions," in *Theory of Complex Functions*, 4th ed., S. Axler and F. W. Gehring, eds. (Springer, 1998), Ch. 11, pp. 321–341.

1. Introduction

The Fabry-Pérot resonator which was invented in 1899 [1] has proven very useful as a high-finesse interferometer in uncountable spectroscopic applications. Since 1960, it has also formed the fundamental basis for a large class of open resonators that have enabled laser oscillation. Lasers with resonator configurations that provide strong light confinement and accordingly high optical gain, such as semiconductor and dielectric channel waveguide lasers, as well as fiber lasers, are particularly successful examples. Due to their high gain, these configurations do not only accommodate high propagation losses and allow for high transmission losses through one of their resonator mirrors, but are in fact often preferably operated with high transmission, because the outcoupling efficiency, i.e., the fraction of useful transmission losses among the overall resonator losses, is one of the key parameters determining the laser slope efficiency. Driven by the quest for miniaturization and mass fabrication, in recent years also various integrated-optical resonator structures with low quality factor Q, be it because of low feedback or high intrinsic losses or both, have emerged. Therefore, low-reflectivity and high-loss Fabry-Pérot resonators have become very common tools nowadays.

The Fabry-Pérot resonator has been extensively investigated, experimentally as well as theoretically. Its theoretical descriptions and proposed approximations and simplifications stem from times when high-finesse spectroscopic applications were dominating and lasers either did not exist or still provided rather low gain, hence necessitating low-loss resonators. However, when the losses become high, discrepancies between the theoretical approaches surface, common approximations turn invalid, and even the definitions of typical parameters break down or prove inappropriate. All these deficiencies go unnoticed when the resonator losses are low. In fact, the class of low-reflectivity and high-loss Fabry-Pérot resonators is not well described by the approximations applied in the common literature.

In this paper, we analyze the performance and relevant parameters of the Fabry-Pérot resonator, with reference to the book on the Fabry-Pérot resonator by Vaughan [2,3] and the standard text books by Siegman [4–7], Svelto [8,9], and Saleh and Teich [10–12]. We demonstrate that the sum of the mode profiles of all longitudinal modes, which are Lorentzian-shaped in case of frequency-independent losses, is the fundamental spectral function that characterizes the Fabry-Pérot resonator. It physically generates the Airy distribution of the Fabry-Pérot resonator, even at low reflectivity and for different or frequency-dependent reflectivities of the two mirrors. Based on this fact, we emphasize that the resonator losses are quantified by the linewidths of the underlying Lorentzian lines and not by the measured Airy linewidth, and we define the Lorentzian finesse which quantifies the resolution of the Lorentzian lines, whereas the usually considered Airy finesse only quantifies the performance of the Fabry-Pérot resonator as a scanning spectrometer. We also point out that the concepts of linewidth and finesse of the Airy distribution of a Fabry-Pérot resonator break down at a mirror-reflectivity product equaling $(0.172)^2$. Moreover, we investigate the influence of frequency-dependent mirror reflectivity, resulting in deformed mode profiles that can be analytically determined.

Optics EXPRESS

2. Resonator losses and outcoupled light

2.1 Definition of resonator losses

Throughout this paper, we assume a two-mirror Fabry-Pérot resonator of geometrical length ℓ, homogeneously filled with a medium of refractive index n_r. Both, ℓ and n_r are assumed to vary insignificantly over the frequency range of interest. The round-trip time t_{RT} of light travelling in the resonator with speed $c = c_0/n_r$, where c_0 is the speed of light in vacuum, is given by

$$t_{RT} = \frac{2\ell}{c}. \tag{1}$$

Generally, this resonator suffers from different optical losses along the light-propagation path. These losses can be of a discrete or continuous nature and usually vary with frequency ν. Discrete outcoupling losses occur due to non-perfect reflectivity of the two mirrors,

$$\begin{aligned} r_i^2 = R_i = 1 - t_{out,i}^2 = 1 - T_{out,i} = e^{-t_{RT}/\tau_{out,i}} = e^{-\delta_{out,i}} \quad \Leftrightarrow \\ \frac{1}{\tau_{out,i}} = \frac{-\ln(R_i)}{t_{RT}} = \frac{-\ln(1-T_{out,i})}{t_{RT}} = \frac{\delta_{out,i}}{t_{RT}} \end{aligned} \tag{2}$$

Here, $r_i(\nu)$ and $R_i(\nu)$ are the electric-field and intensity reflectivities, respectively, $t_{out,i}(\nu)$ and $T_{out,i}(\nu)$ are the electric-field and intensity transmissions, respectively, and $\tau_{out,i}(\nu)$ is the exponential decay time resulting from the outcoupling loss at mirror i. Siegman [4] and others named the ratios $\delta_{out,i}(\nu)$ the "mirror coupling coefficients", referred to as the "delta notation".

Other discrete losses are, e.g., diffraction losses at the mirrors of finite lateral dimensions, absorption and scattering losses in the mirror coatings, diffraction losses at the edges of an active laser medium that is shorter than the resonator length, or losses due to other optical elements inside the resonator. Furthermore, continuous intensity losses per unit length may be induced by the medium, e.g. scattering losses due to material imperfections, waveguide propagation losses due to interface roughness, or absorption losses. All these losses shall be neglected in this paper, because they do not change the fundamental findings presented here. The photon-decay time $\tau_c(\nu)$ of the resonator is then given by

$$\frac{1}{\tau_c} = \sum_i \frac{1}{\tau_{out,i}} = \frac{\sum_i \delta_{out,i}}{t_{RT}} = \frac{\sum_i -\ln(R_i)}{t_{RT}}. \tag{3}$$

Traditionally, the index c in τ_c stands for "cavity" which means the resonator. In this paper, it is used for quantities in the spectral domain that relate to the exponential decay time τ_c of light coupled out of the resonator, namely the spectral linewidth $\Delta\nu_c$ of the Lorentzian lines (Section 2.3) and the Lorentzian finesse F_c (Section 4.1).

In the two subsequent Sections 3 and 4, the outcoupling losses are assumed to be independent of frequency. The case in which τ_c varies with frequency due to a frequency dependence of the mirror reflectivities R_i is treated in Section 5.

2.2 Photon decay

The resonator can be investigated by inserting light as a short pulse or continuously. In the transient regime, the number $\varphi(t)$ of photons at frequency ν, present inside the resonator at time t, is described via the photon-decay time $\tau_c(\nu)$ by the differential rate equation

$$\frac{d}{dt}\varphi(t) = -R_{decay}(t) = -\frac{1}{\tau_c}\varphi(t). \tag{4}$$

Optics EXPRESS

$R_{decay}(t)$ is the photon-decay rate per unit time. With a number φ_s of photons present at the starting time $t = 0$, integration delivers

$$\varphi(t) = \varphi_s e^{-t/\tau_c}. \tag{5}$$

The change of $\varphi(t)$ per round trip is described by the integral round-trip equation

$$\varphi(t + t_{RT}) = \varphi(t) e^{-t_{RT}/\tau_c} = \varphi(t) R_1 R_2. \tag{6}$$

In contrast, a steady-state or continuous-wave (cw) regime where the decaying photon number is continuously replenished by the incoupling of photons from an external source, such that $\varphi(t) = \varphi_s$ at all times, is described by the equation

$$R_{decay} \overset{cw}{=} \frac{1}{\tau_c} \varphi_s. \tag{7}$$

Consequently, the number φ_{decay} of photons lost during a time interval Δt in the transient and cw regime,

$$\varphi_{decay}(\Delta t) \overset{transient}{=} \int_{t=0}^{t=\Delta t} R_{decay}(t)\, dt = \int_{t=0}^{t=\Delta t} \frac{1}{\tau_c} \varphi_s e^{-t/\tau_c} dt = \varphi_s \left(1 - e^{-\Delta t/\tau_c}\right) \overset{\Delta t = \tau_c}{=} \varphi_s \left(1 - e^{-1}\right), \tag{8}$$

$$\varphi_{decay}(\Delta t) \overset{cw}{=} \int_{t=0}^{t=\Delta t} R_{decay}\, dt = \frac{\Delta t}{\tau_c} \varphi_s \overset{\Delta t = \tau_c}{=} \varphi_s, \tag{9}$$

respectively, are different. Whereas in the transient regime the photon number in the resonator decays to the fraction e^{-1} of its original value during the photon-decay time τ_c, in the cw regime in average all photons are lost during τ_c, because additionally the photons that are replenished during τ_c contribute to the decay during τ_c.

2.3 Resonance frequencies, free spectral range, and spectral line shapes

With $\phi(\nu)$ quantifying the single-pass phase shift between the mirrors, the round-trip phase shift at frequency ν accumulates to

$$2\phi(\nu) = 2\pi\nu t_{RT} = 2\pi\nu \frac{2\ell}{c}. \tag{10}$$

The geometrical length ℓ of an ideal two-mirror Fabry-Pérot resonator is independent of frequency. For simplicity, we have assumed at the beginning of Section 2 that also the refractive index n_r of its medium and, thus, the speed of light c are independent of frequency. Consequently, also the round-trip time t_{RT} becomes independent of frequency. Resonances occur at frequencies at which light exhibits constructive interference after one round trip. The difference in phase shift per round trip between adjacent resonance frequencies amounts to 2π, from which the free spectral range $\Delta\nu_{FSR}$ then derives as [3]

$$\frac{d}{d\nu}(2\phi) = \frac{d}{d\nu}(2\pi\nu t_{RT}) = 2\pi t_{RT} \;\Rightarrow\; \frac{2\pi}{\Delta\nu_{FSR}} = 2\pi t_{RT} \;\Rightarrow\; \Delta\nu_{FSR} = \frac{1}{t_{RT}}. \tag{11}$$

Each resonator mode with its mode index q, where q is an integer number in the interval $[-\infty, \ldots, -1, 0, 1, \ldots, \infty]$, is associated with a resonance frequency ν_q and wavenumber k_q,

$$\nu_q = q\Delta\nu_{FSR} = q/t_{RT} \;\Rightarrow\; k_q = \frac{2\pi q \Delta\nu_{FSR}}{c}. \tag{12}$$

Optics EXPRESS

Two modes with opposite values ± q and ± k of modal index and wavenumber, respectively, physically representing opposite propagation directions, occur at the same absolute value $|\nu_q|$ of frequency.

According to Eq. (5), light at frequency ν oscillating inside the resonator decays out of the resonator with a time constant of $\tau_c(\nu)$. If the resonator losses are independent of frequency, the photon-decay time $\tau_c(\nu)$ is the same at all frequencies. The decaying electric field at frequency ν_q is represented by a damped harmonic oscillation with an initial amplitude of $E_{q,s}$ and a decay-time constant of $2\tau_c$. In phasor notation, it can be expressed as

$$E_q(t)=\begin{cases} E_{q,s}e^{i2\pi\nu_q t}e^{-t/(2\tau_c)} & t\ge 0 \\ 0 & t<0 \end{cases}. \tag{13}$$

Fourier transformation of the electric field in time provides the electric field per unit frequency interval,

$$\tilde{E}_q(\nu)=\int_{-\infty}^{+\infty}E_q(t)e^{-i2\pi\nu t}dt=E_{q,s}\int_0^{+\infty}e^{-\left[1/(2\tau_c)+i2\pi(\nu-\nu_q)\right]t}dt=E_{q,s}\frac{1}{(2\tau_c)^{-1}+i2\pi(\nu-\nu_q)}. \tag{14}$$

Each mode has a normalized spectral line shape per unit frequency interval given by [13]

$$\begin{aligned}\tilde{\gamma}_q(\nu)&=\frac{1}{\tau_c}\left|\frac{\tilde{E}_q(\nu)}{E_{q,s}}\right|^2=\frac{1}{\tau_c}\left|\frac{1}{(2\tau_c)^{-1}+i2\pi(\nu-\nu_q)}\right|^2=\frac{1}{\tau_c}\frac{1}{(2\tau_c)^{-2}+4\pi^2(\nu-\nu_q)^2}, \\ &=\frac{1}{\pi}\frac{1/(4\pi\tau_c)}{1/(4\pi\tau_c)^2+(\nu-\nu_q)^2}\quad\text{with}\quad\int\tilde{\gamma}_q(\nu)d\nu=1\end{aligned} \tag{15}$$

in units of (1/Hz). The calibration factor $1/\tau_c$ in Eq. (15) compensates for the broadening of the Lorentzian line as the photon-decay time becomes shorter, such that the integral of the Lorentzian line is normalized to unity. Introducing the full-width-at-half-maximum (FWHM) linewidth $\Delta\nu_c$ of the Lorentzian spectral line shape, we obtain

$$\Delta\nu_c=\frac{1}{2\pi\tau_c}\ \Rightarrow\ \tilde{\gamma}_q(\nu)=\frac{1}{\pi}\frac{\Delta\nu_c/2}{(\Delta\nu_c/2)^2+(\nu-\nu_q)^2}\quad\text{with}\quad\int\tilde{\gamma}_q(\nu)d\nu=1. \tag{16}$$

Calibrated to a peak height of unity, we obtain the Lorentzian lines, in units of (1):

$$\gamma_{q,L}(\nu)=\frac{\pi}{2}\Delta\nu_c\tilde{\gamma}_q(\nu)=\frac{(\Delta\nu_c)^2}{(\Delta\nu_c)^2+4(\nu-\nu_q)^2}\quad\text{with}\quad\gamma_{q,L}(\nu_q)=1. \tag{17}$$

When repeating the above Fourier transformation for all the modes with mode index q in the resonator, one obtains the full mode spectrum of the resonator.

3. Airy distributions of the Fabry-Pérot resonator

In this Section, we demystify the Airy distribution. We derive the generic Airy distribution, show that it represents the spectral dependence of the internal resonant enhancement factor, and demonstrate that all other Airy distributions describing the circulating, back-circulating, transmitted, and back-transmitted intensity (Fig. 1) only include simple scaling factors, depending on whether the light incident upon mirror 1 or its fraction launched into the resonator is considered as a reference. Most importantly, we verify that the physical origin of the Airy distribution is the sum of mode profiles of the longitudinal resonator modes.

Optics EXPRESS

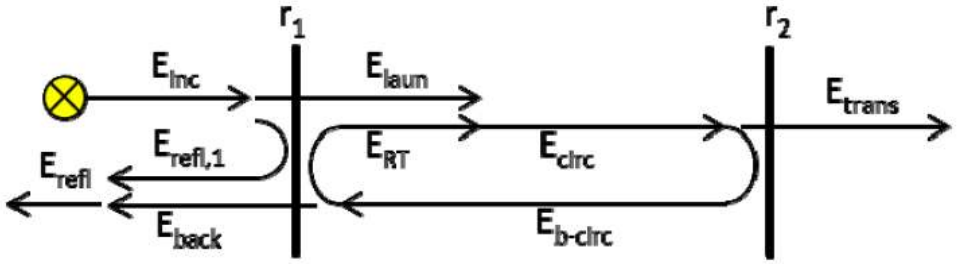

Fig. 1. Fabry-Pérot resonator with electric-field mirror reflectivities r_1 and r_2. Indicated are the characteristic electric fields produced by an electric field E_{inc} incident upon mirror 1: $E_{refl,1}$ initially reflected at mirror 1, E_{laun} launched through mirror 1, E_{circ} and $E_{b\text{-}circ}$ circulating inside the resonator in forward and backward propagation direction, respectively, E_{RT} propagating inside the resonator after one round trip, E_{trans} transmitted through mirror 2, E_{back} transmitted through mirror 1, and the total field E_{refl} propagating backward. Interference occurs at the left- and right-hand sides of mirror 1 between $E_{refl,1}$ and E_{back}, resulting in E_{refl}, and between E_{laun} and E_{RT}, resulting in E_{circ}, respectively.

3.1 Generic Airy distribution: The internal resonance enhancement factor

The response of the Fabry-Pérot resonator is most easily derived by use of the circulating-field approach [5], as displayed in Fig. 1. This approach assumes a steady state and derives the Airy distributions via the electric field E_{circ} circulating inside the resonator. In fact, E_{circ} is the field propagating in the forward direction from mirror 1 to mirror 2 after interference between the field E_{RT} that is circulating after one round trip, i.e., after having suffered outcoupling losses at both mirrors, and the field E_{laun} launched through the first mirror.

With the phase shift 2ϕ of Eq. (10) accumulated in one round trip, the field E_{circ} can be related to the field E_{laun} that is launched into the resonator in the situation of Fig. 1(a) by

$$E_{circ} = E_{laun} + E_{RT} = E_{laun} + r_1 r_2 e^{-i2\phi} E_{circ} \quad \Rightarrow \quad \frac{E_{circ}}{E_{laun}} = \frac{1}{1 - r_1 r_2 e^{-i2\phi}}. \tag{18}$$

The generic Airy distribution, which considers solely the physical processes exhibited by light inside the resonator, then derives as the intensity circulating in the resonator relative to the intensity launched, which by use of Eqs. (56)-(57) of Appendix A yields

$$A_{circ} = \frac{I_{circ}}{I_{laun}} = \frac{\left|E_{circ}\right|^2}{\left|E_{laun}\right|^2} = \frac{1}{\left|1 - r_1 r_2 e^{-i2\phi}\right|^2} = \frac{1}{\left(1 - \sqrt{R_1 R_2}\right)^2 + 4\sqrt{R_1 R_2}\sin^2(\phi)}. \tag{19}$$

Physically, A_{circ} represents the spectrally dependent internal resonance enhancement which the resonator provides to the light launched into it. It is displayed for different mirror reflectivities in Fig. 2. At the resonance frequencies ν_q, where $\sin(\phi)$ equals zero, the internal resonance enhancement factor is

$$A_{circ}(\nu_q) = \frac{1}{\left(1 - \sqrt{R_1 R_2}\right)^2}. \tag{20}$$

Optics EXPRESS

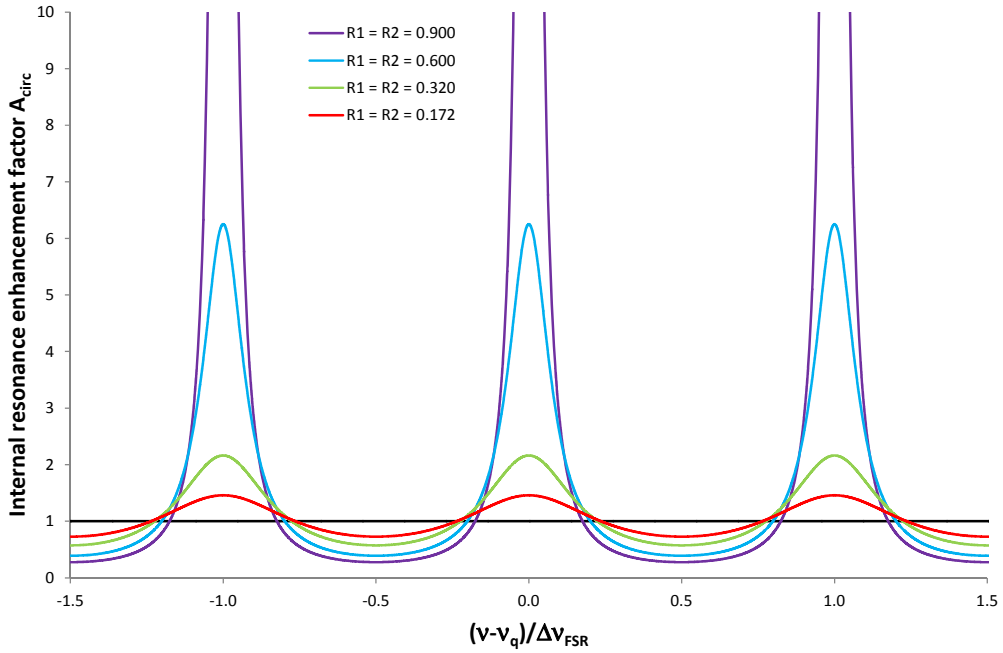

Fig. 2. Generic Airy distribution A_{circ}, equaling the spectrally dependent internal resonance enhancement which the resonator provides to light that is launched into it. For the curve with $R_1 = R_2 = 0.9$, the peak value is at $A_{circ}(\nu_q) = 100$, outside the scale of the ordinate.

The internal resonance enhancement factor A_{circ} integrated over one free spectral range, i.e., 2ϕ in the interval $[-\pi, \ldots \pi]$ or ϕ in the interval $[-\pi/2, \ldots \pi/2]$, is (see Appendix B)

$$A_{FSR} = \frac{1}{\pi}\int_{-\pi/2}^{+\pi/2} A_{circ}\, d\phi = \frac{1}{1-R_1R_2}. \tag{21}$$

The integral resonance enhancement A_{FSR} is displayed as a function of R_1R_2 in Fig. 3(a).

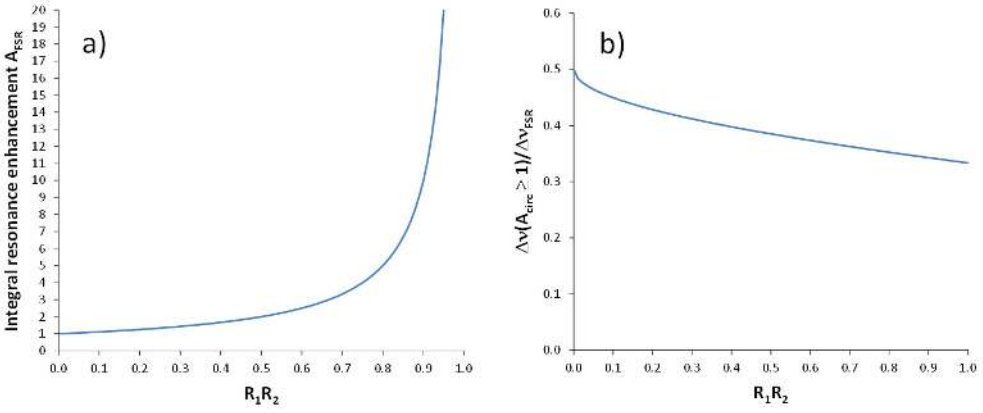

Fig. 3. (a) Integral resonance enhancement A_{FSR} (integrated over one free spectral range) and (b) fraction of the free spectral range over which enhancement occurs, i.e., $A_{circ} \geq 1$, as a function of the product of mirror reflectivities, R_1R_2.

As can be seen in Fig. 2, the fraction of the free spectral range over which enhancement of light occurs, narrows with increasing reflectivities. From Eq. (19), this fraction derives as

Optics EXPRESS

$$A_{circ} \geq 1 \Rightarrow \sin(\phi) \leq \frac{1}{2}\sqrt{2-\sqrt{R_1 R_2}} \Rightarrow \frac{\Delta\nu_{A_{circ}\geq 1}}{\Delta\nu_{FSR}} = \frac{2}{\pi}\arcsin\left(\frac{1}{2}\sqrt{2-\sqrt{R_1 R_2}}\right). \quad (22)$$

The fraction is displayed in Fig. 3(b). The spectral range of enhancement decreases from $\Delta\nu_{FSR}/2$ for $R_1R_2 = 0$ to $\Delta\nu_{FSR}/3$ for $R_1R_2 \to 1$.

3.2 Other Airy distributions

Once the internal resonance enhancement, the generic Airy distribution of Eq. (19), is established, all other Airy distributions, i.e., the observed light intensities relative to the launched or initial intensity from the light source (Fig. 1) can then be straight-forwardly deduced by simple scaling factors. Since the intensity launched into the resonator equals the transmitted fraction of the intensity incident upon mirror 1,

$$I_{laun} = (1-R_1) I_{inc}, \quad (23)$$

and the intensities transmitted through mirror 2, reflected at mirror 2, and transmitted through mirror 1 are the transmitted and reflected/transmitted fractions of the intensity circulating inside the resonator,

$$I_{trans} = (1-R_2) I_{circ}, \quad I_{b-circ} = R_2 I_{circ}, \quad I_{back} = (1-R_1) I_{b-circ}, \quad (24)$$

respectively, one obtains the following Airy distributions:

$$A_{b\text{-}circ} = \frac{I_{b\text{-}circ}}{I_{laun}} = R_2 A_{circ}, \quad (25)$$

$$A_{trans} = \frac{I_{trans}}{I_{laun}} = (1-R_2) A_{circ}, \quad (26)$$

$$A_{back} = \frac{I_{back}}{I_{laun}} = (1-R_1) R_2 A_{circ}, \quad (27)$$

$$A_{emit} = A_{trans} + A_{back} = \frac{I_{trans} + I_{back}}{I_{laun}} = (1-R_1R_2) A_{circ}, \quad (28)$$

$$A'_{circ} = \frac{I_{circ}}{I_{inc}} = (1-R_1) A_{circ}, \quad (29)$$

$$A'_{b\text{-}circ} = \frac{I_{b\text{-}circ}}{I_{inc}} = (1-R_1) R_2 A_{circ}, \quad (30)$$

$$A'_{trans} = \frac{I_{trans}}{I_{inc}} = (1-R_1)(1-R_2) A_{circ}, \quad (31)$$

$$A'_{back} = \frac{I_{back}}{I_{inc}} = (1-R_1)^2 R_2 A_{circ}, \quad (32)$$

$$A'_{emit} = A'_{trans} + A'_{back} = \frac{I_{trans} + I_{back}}{I_{inc}} = (1-R_1)(1-R_1R_2) A_{circ}. \quad (33)$$

The index “emit” denotes Airy distributions that consider the sum of intensities emitted on both sides of the resonator. The prime denotes Airy distributions with respect to the incident intensity I_{inc}.

Optics EXPRESS

The back-transmitted intensity I_{back} cannot be measured, because also the initially back-reflected light adds to the backward-propagating signal. The measurable case of the intensity resulting from the interference of both backward-propagating electric fields is treated in Appendix A. At the resonance frequencies, the back-emitted electric field E_{back} destructively interferes with the electric field $E_{refl,1}$ initially back-reflected.

Like A_{circ} represents the internal resonance enhancement factor with respect to I_{laun}, A'_{circ} of Eq. (29) represents the external resonance enhancement factor with respect to I_{inc}. The external resonance enhancement factor at the resonance frequencies, $A'_{circ}(\nu_q)$, and integrated over one free spectral range, A'_{FSR}, respectively, are

$$A'_{circ}(\nu_q) = \frac{(1-R_1)}{\left(1-\sqrt{R_1R_2}\right)^2} = (1-R_1)\,A_{circ}(\nu_q) \quad \text{and} \quad A'_{FSR} = (1-R_1)\,A_{FSR}. \qquad (34)$$

I.e., the distributions A'_{circ}, $A'_{circ}(\nu_q)$, and A'_{FSR} related to the incident light are smaller by the same factor $1-R_1$ than the same distributions related to the launched light, because only this fraction $1-R_1$ of the light incident on mirror 1 is transmitted into the resonator, see Eq. (23).

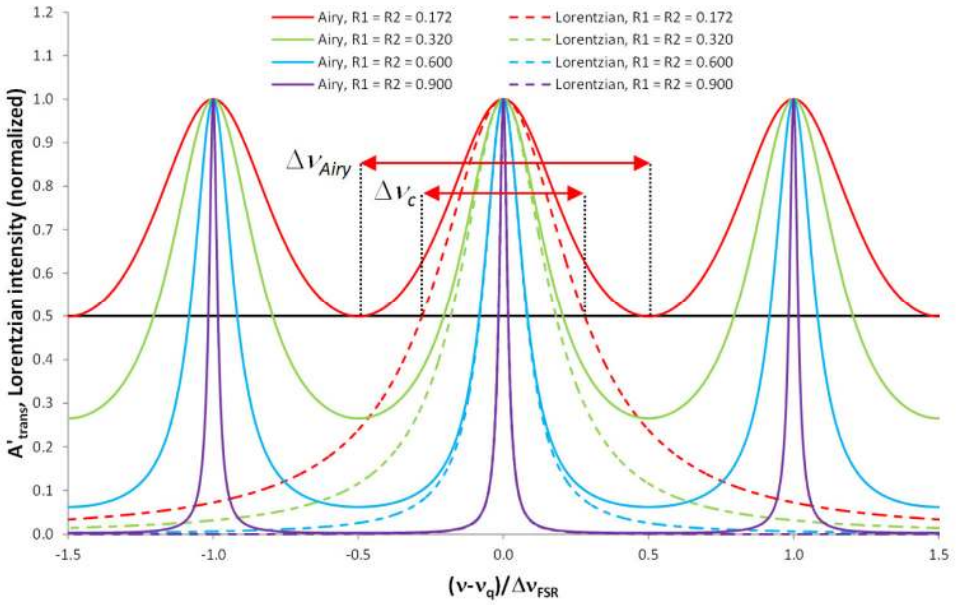

Fig. 4. Airy distribution A'_{trans} (solid lines), corresponding to light transmitted through a Fabry-Pérot resonator, calculated from Eq. (31) for different values of the reflectivities $R_1 = R_2$, and comparison with a single Lorentzian line (dashed lines) calculated from Eq. (17) for the same $R_1 = R_2$. At half maximum (black line), with decreasing reflectivities the FWHM linewidth $\Delta\nu_{Airy}$ of the Airy distribution broadens compared to the FWHM linewidth $\Delta\nu_c$ of its corresponding Lorentzian line: $R_1 = R_2 = 0.9$, 0.6, 0.32, 0.172 results in $\Delta\nu_{Airy} / \Delta\nu_c = 1.001$, 1.022, 1.132, 1.717, respectively.

In experimental situations, often light is transmitted through a Fabry-Pérot resonator in order to characterize the resonator or to use it as a scanning interferometer (see later in Section 4). Therefore, an often applied Airy distribution is A'_{trans} of Eq. (31). It describes the fraction I_{trans} of the intensity I_{inc} of a light source incident upon mirror 1 that is transmitted through mirror 2, see Fig. 1. A'_{trans} is displayed in Fig. 4 (solid lines) for different values of the reflectivities $R_1 = R_2$. Its peak value at the resonance frequencies ν_q is

Optics EXPRESS

$$A'_{trans}\left(\nu_q\right)=\frac{\left(1-R_1\right)\left(1-R_2\right)}{\left(1-\sqrt{R_1R_2}\right)^2}\overset{R_1=R_2}{=}1. \tag{35}$$

A'_{trans} has been derived in the circulating-field approach [5] by considering an additional phase shift of $e^{i\pi/2}=i$ during each transmission through a mirror (alternatively, but equivalently, often a phase shift of $e^{i\pi}=-1$ during reflection from the low-refractive-index side of a mirror is assumed) [7] and by use of Eqs. (56)-(58) of Appendix A:

$$E_{circ}=it_1E_{inc}+r_1r_2e^{-i2\phi}E_{circ}\ \Rightarrow\ \frac{E_{circ}}{E_{inc}}=\frac{it_1}{1-r_1r_2e^{-i2\phi}}, \tag{36}$$

$$E_{trans}=it_2E_{circ}e^{-i\phi}\ \Rightarrow\ \frac{E_{trans}}{E_{inc}}=\frac{-t_1t_2e^{-i\phi}}{1-r_1r_2e^{-i2\phi}}, \tag{37}$$

$$A'_{trans}=\frac{I_{trans}}{I_{inc}}=\frac{\left|E_{trans}\right|^2}{\left|E_{inc}\right|^2}=\frac{\left|-t_1t_2e^{-i\phi}\right|^2}{\left|1-r_1r_2e^{-i2\phi}\right|^2}=\frac{\left(1-R_1\right)\left(1-R_2\right)}{\left(1-\sqrt{R_1R_2}\right)^2+4\sqrt{R_1R_2}\sin^2\left(\phi\right)}, \tag{38}$$

which equals Eq. (31). Alternatively, it can be obtained via the round-trip-decay approach [8] by tracing the infinite number of round trips that the incident electric field E_{inc} exhibits after entering the resonator and accumulating the electric field E_{trans} transmitted in all round trips. The field transmitted after the first propagation and the smaller and smaller fields transmitted after each consecutive propagation through the resonator are

$$E_{trans,1}=E_{inc}it_1it_2e^{-i\phi}=-E_{inc}t_1t_2e^{-i\phi}\ \text{ and }\ E_{trans,m+1}=E_{trans,m}r_1r_2e^{-i2\phi}, \tag{39}$$

respectively. Exploiting

$$\sum_{m=0}^{\infty}x^m=\frac{1}{1-x}\ \Rightarrow\ E_{trans}=\sum_{m=1}^{\infty}E_{trans,m}=-E_{inc}t_1t_2e^{-i\phi}\sum_{m=0}^{\infty}\left(r_1r_2\right)^m e^{-im2\phi}=E_{inc}\frac{-t_1t_2e^{-i\phi}}{1-r_1r_2e^{-i2\phi}}. \tag{40}$$

This result is identical to Eq. (37), therefore one obtains the same Airy distribution of Eq. (38). Svelto [8] uses the alternative convention for the phase shift occurring at the mirrors, hence obtains no minus sign in the numerator of Eq. (40), which becomes irrelevant when squaring the electric field to calculate the intensity. A'_{trans} has also been derived in the impulse-response approach [14]. This approach is identical to the round-trip-decay approach [8], except that it assumes a specific light source that has a delta function in time, which Fourier transforms to an infinite frequency spectrum, such that A'_{trans} is probed over the entire spectral range.

3.3 Airy distribution as a sum of mode profiles

In Fig. 4 one observes that, at high reflectivity, there is almost perfect agreement between the spectral shape of the Airy distribution (solid purple line) and its underlying Lorentzian lines (dashed purple line), i.e., the former is rather well represented by the latter. This fact has prompted Saleh and Teich [10] to propose that in this case the Airy linewidth $\Delta\nu_{Airy}$ of a Fabry-Pérot resonator is similar to the linewidth $\Delta\nu_c = 1/(2\pi\tau_c)$ of its underlying Lorentzian lines, both defined as FWHM (black line). However, as is generally well known, with decreasing reflectivity the linewidth of the Airy distribution (solid lines) broadens faster than that of the underlying Lorentzian lines (dashed lines).

Svelto [9] attributes this discrepancy to Eq. (5) being only an approximation, thereby implicating that also Eq. (15) is only an approximation, such that the Airy linewidth $\Delta\nu_{Airy}$ of

Optics EXPRESS

a Fabry-Pérot resonator can only at high reflectivity be approximated by the linewidth Δv_c of its underlying Lorentzian lines. We will demonstrate that the discrepancy has a different reason.

According to Koppelmann [15], Bayer-Helms [16] "showed that the Airy distribution can be represented exactly" by the sum of Lorentzian spectral line shapes times a calibration factor. Firstly, while being literally correct, this statement is physically misleading, secondly, the calibration factor used in [15] remains unexplained, thirdly, the equivalence is shown only for equal reflectivities, $R_1 = R_2$, and finally, the equivalence is not investigated for non-Lorentzian spectral line shapes. Kumer and Uplinger [17] compared the sum of Lorentzian spectral line shapes to an Airy distribution that is different from Eq. (19) and Eq. (31) and, not surprisingly, these authors found a difference.

Here we verify that the Airy distribution is nothing else but the sum of the mode profiles of the longitudinal resonator modes, thereby revealing the physical origin of the Airy distribution. Our approach starts from the electric field E_{circ} circulating inside the resonator, considers the exponential decay in time of this field through both mirrors of the resonator, see Fig. 1, Fourier transforms it to frequency space according to Eq. (14) to obtain the normalized spectral line shapes $\tilde{\gamma}_q(\nu)$ of Eq. (15), divides it by the round-trip time t_{RT} to account for how the total circulating electric-field intensity is longitudinally distributed in the resonator and coupled out per unit time, resulting in the emitted mode profiles,

$$\gamma_{q,emit}(\nu) = \frac{1}{t_{RT}} \tilde{\gamma}_q(\nu), \tag{41}$$

in units of (1), and then sums over the emitted mode profiles of all longitudinal modes at positive, zero, and negative frequencies. Consequently, the sum of emitted mode profiles describes an experiment that must result in the Airy distribution A_{emit} of Eq. (28). Exploiting the derivation given in Eqs. (64)-(72) of Appendix C, the sum of emitted mode profiles of Eq. (41) yields

$$\sum_{q=-\infty}^{\infty} \gamma_{q,emit}(\nu) = \frac{1-R_1R_2}{\left(1-\sqrt{R_1R_2}\right)^2 + 4\sqrt{R_1R_2}\sin^2(\phi)} = A_{emit}, \tag{42}$$

which is indeed equal to Eq. (28), with Eq. (19) inserted. Each spectral line shape $\tilde{\gamma}_q(\nu)$ of Eq. (15) and mode profile $\gamma_{q,emit}(\nu)$ of Eq. (41) is extended over the infinite frequency range, consequently light at a specific frequency v inside the resonator excites all longitudinal modes of the resonator. However, the contributions from different longitudinal modes to the light at frequency v do not interfere with each other, because all optical modes are orthogonal with each other. For this reason, the sum in Eq. (42) is over the intensity mode profiles $\gamma_{q,emit}(\nu)$ rather than over the electric fields. Because of resonant enhancement of the launched light the peak value of A_{emit} at the resonance frequencies v_q,

$$A_{emit}(\nu_q) = \frac{1-R_1R_2}{\left(1-\sqrt{R_1R_2}\right)^2} = \frac{1+\sqrt{R_1R_2}}{1-\sqrt{R_1R_2}} > 1, \tag{43}$$

becomes larger than unity. Nevertheless, because of Eqs. (23) and (59) the energy of the system is conserved.

The observation that with decreasing R_1 and R_2 the linewidth of the resulting Airy distribution in Fig. 4 is increasingly broader than the linewidth of the underlying Lorentzian lines simply arises from the fact that one sums up mode profiles (with the same linewidth as the Lorentzian lines) that resonate at different frequencies. It does not constitute a discrepancy, as has often been proposed.

Optics EXPRESS

The derivation shown here demonstrates that—from a physical point of view—the spectral line shapes and mode profiles are the fundamental spectral functions that characterize the Fabry-Pérot resonator and their sum quantifies its spectral response. The circulating-field and round-trip-decay approaches only implicitly exploit this fact, thereby obscuring the physical nature of the Airy distribution. As we will see in Section 4, this fundamental understanding has direct consequences for the definitions of linewidth and finesse.

The same simple scaling factors of Eqs. (23) and (24) that provide the relations between the individual Airy distributions, see Eqs. (19) and (25)-(33), also provide the relations among $\gamma_{q,emit}(\nu)$ and the other mode profiles:

$$\begin{aligned}\gamma_{q,circ} &= \frac{1}{R_2}\gamma_{q,b\text{-}circ} = \frac{1}{1-R_2}\gamma_{q,trans} = \frac{1}{1-R_1}\gamma_{q,back} = \frac{1}{1-R_1R_2}\gamma_{q,emit} \\ \gamma'_{q,circ} &= \frac{1}{R_2}\gamma'_{q,b\text{-}circ} = \frac{1}{1-R_2}\gamma'_{q,trans} = \frac{1}{1-R_1}\gamma'_{q,back} = \frac{1}{1-R_1R_2}\gamma'_{q,emit} = (1-R_1)\,\gamma_{q,circ}.\end{aligned} \tag{44}$$

The various mode profiles $\gamma_q(\nu)$ and $\gamma'_q(\nu)$ are calibrated with respect to the launched and the incident intensity, respectively, and the sum over one of these mode profiles at all resonance frequencies generates the corresponding Airy distribution.

3.4 0th-order mode: no cut-off wavelength!

The resonance frequencies of the Fabry-Pérot resonator are given by Eq. (12). Particularly, $q = 0$, resulting in $\nu_q = 0$, is a physical solution of Eq. (12), and the mode profiles summed in Eq. (42) include this 0th-order mode [18]. Consequently, in wavelength space there exists no cut-off wavelength at the resonance line with $q = 1$, but an additional resonance occurs at infinite wavelength. As long as the resonator losses are low (purple line in Fig. 5), in most cases this resonance will go unnoticed. However, when the losses become significant and the mode profiles broaden, this resonance manifests itself in a steady increase of the Airy distribution A'_{trans} in the long-wavelength range (other lines in Fig. 5). While this effect looks quite dramatic in Fig. 5, one should keep in mind that the natural energy or frequency units are, when converted to wavelength units, expanded by λ^2 at the long-wavelength side.

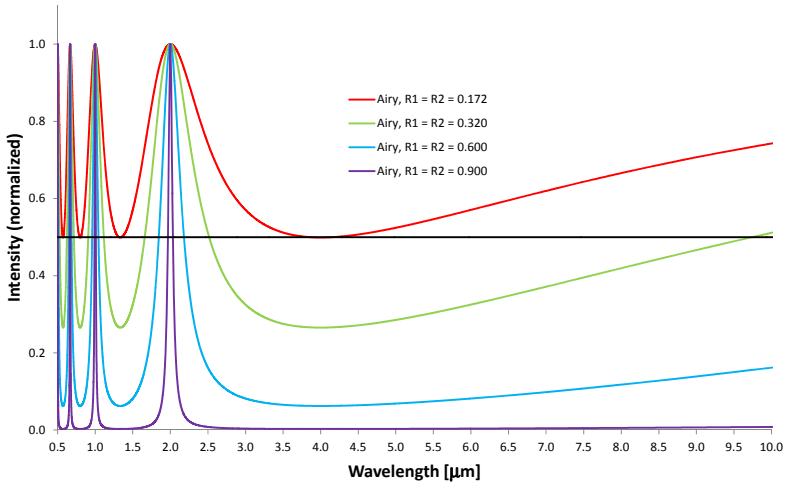

Fig. 5. Airy distribution A'_{trans} of a Fabry-Pérot micro-resonator with a length of ℓ = 1 µm versus wavelength, calculated from Eq. (31) for different values of the reflectivities $R_1 = R_2$. The resonance peak with $q = 1$, in our example occurring at a wavelength of 2 µm, which is often considered as a "cut-off wavelength". At wavelengths beyond 4 µm, however, the Airy distribution increases towards the resonance peak with $q = 0$, located at infinite wavelength.

Optics EXPRESS

4. Lorentzian linewidth and finesse versus Airy linewidth and finesse

The most commonly accepted definitions of spectral resolution are the Rayleigh criterion and the Taylor criterion. The Rayleigh criterion [19] applies to diffraction spots and proposes that two intensity maxima can be resolved if the maximum of the first spot is spectrally superimposed on the first minimum of the second spot. For spectral lines that do not exhibit minima, such as the Lorentzian lines underlying the Airy distribution of a Fabry-Pérot resonator, as well as the Airy distribution itself within one free spectral range from $\nu_q - \Delta\nu_{FSR}/2$ to $\nu_q + \Delta\nu_{FSR}/2$, the Taylor criterion [20] is more appropriate. It proposes that two spectral lines can be resolved if the individual lines cross at half intensity. In the case of two identical, symmetric spectral lines their peaks would then be separated by their FWHM. The Taylor criterion is utilized in the following.

Optics EXPRESS

4.1 Characterizing the Fabry-Pérot resonator: Lorentzian linewidth and finesse

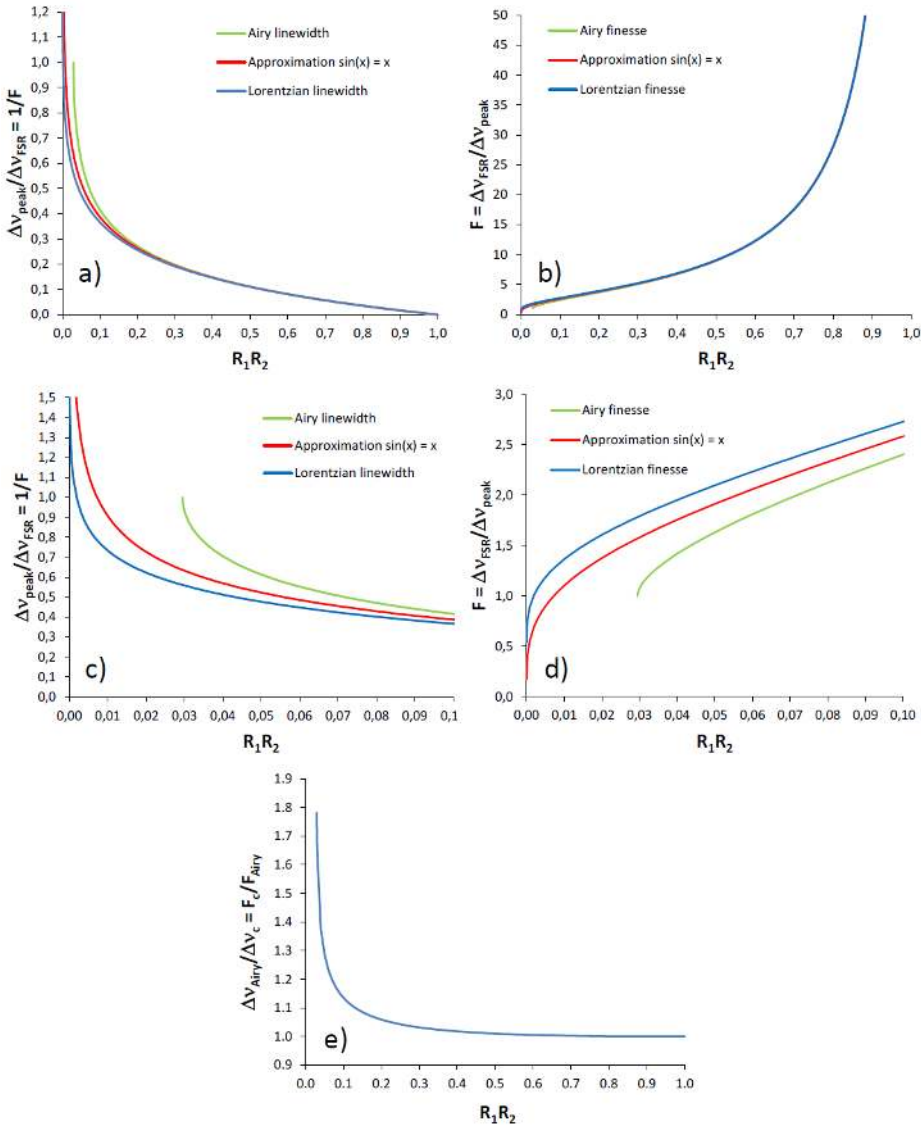

Fig. 6. (a) Relative Lorentzian linewidth $\Delta\nu_c/\Delta\nu_{FSR}$, with $\Delta\nu_c$ from Eq. (16) (blue curve), relative Airy linewidth $\Delta\nu_{Airy}/\Delta\nu_{FSR}$, with $\Delta\nu_{Airy}$ from Eq. (48) (green curve), and its approximation of Eq. (51) (red curve), and (b) Lorentzian finesse F_c of Eq. (45) (blue curve), Airy finesse F_{Airy} of Eq. (50) (green curve), and its approximation of Eq. (52) (red curve) as a function of reflectivity value R_1R_2. (c), (d) Zoom into the low-reflectivity region. The exact solutions of the Airy linewidth and finesse (green lines) correctly break down at $\Delta\nu_{Airy} = \Delta\nu_{FSR}$, equivalent to $F_{Airy} = 1$, whereas their approximations (red lines) incorrectly do not break down. (e) Ratio between the Airy linewidth $\Delta\nu_{Airy}$ of Eq. (48) and the Lorentzian linewidth $\Delta\nu_c$ of Eq. (16), equaling the ratio between the Lorentzian finesse F_c of Eq. (45) and the Airy finesse F_{Airy} of Eq. (50), as a function of reflectivity value R_1R_2.

When launching light into the Fabry-Pérot resonator in a non-scanning experiment, i.e., at fixed resonator length (and fixed angle of incidence), the Fabry-Pérot resonator becomes the object of investigation. The spectral line shapes, Lorentzian lines, and mode profiles are the fundamental functions. By measuring the sum of mode profiles, the Airy distribution, one can

Optics EXPRESS

derive the total loss of the Fabry-Pérot resonator via recalculating the Lorentzian linewidth $\Delta\nu_c$ of Eq. (16), displayed (blue line) relative to the free spectral range in Figs. 6(a) and 6(c).

The underlying Lorentzian lines can be resolved as long as the Taylor criterion is obeyed (Fig. 7). Consequently, one can define a parameter which we call the Lorentzian finesse of a Fabry-Pérot resonator:

$$F_c := \frac{\Delta\nu_{FSR}}{\Delta\nu_c} = \frac{2\pi}{-\ln(R_1 R_2)}. \tag{45}$$

It is displayed as the blue line in Figs. 6(b) and 6(d). This parameter has received little attention in the scientific literature, other than that at high reflectivity, where $\Delta\nu_{Airy} \approx \Delta\nu_c$, see the purple line in Fig. 4, it can serve as a reasonable approximation of the Airy finesse F_{Airy} (see Section 4.2). Yet, the Lorentzian finesse F_c has a fundamental physical meaning: it describes how well the Lorentzian lines underlying the Airy distribution can be resolved when measuring the Airy distribution. A Fabry-Pérot resonator generating single-longitudinal-mode laser light is characterized by its Lorentzian linewidth and finesse.

Since $\Delta\nu_c$ exists for any mirror reflectivity, the definition of the Lorentzian finesse does not break down at a critical value. However, at the point where

$$\Delta\nu_c = \Delta\nu_{FSR} \quad \Rightarrow \quad R_1 R_2 = e^{-2\pi} \approx 0.001867, \tag{46}$$

equivalent to $F_c = 1$, the Taylor criterion for the spectral resolution of a single Airy distribution is reached. For equal mirror reflectivities, this point occurs when $R_1 = R_2 \approx 4.32\%$. Therefore, the linewidth of the Lorentzian lines underlying the Airy distribution of a Fabry-Pérot resonator can be resolved by measuring the Airy distribution, hence its resonator losses can be spectroscopically determined, until this point. Obviously, the Lorentzian finesse according to the definition of Eq. (45) plays an essential role in the characterization of low-reflectivity or otherwise high-loss Fabry-Pérot resonators.

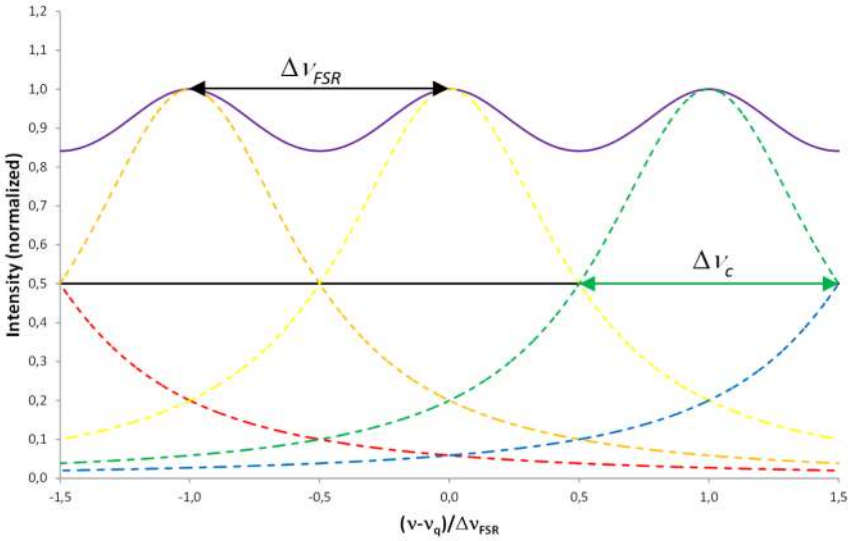

Fig. 7. Illustration of the physical meaning of the Lorentzian finesse F_c of a Fabry-Pérot resonator. Displayed is the situation for $R_1 = R_2 \approx 4.32\%$, at which $\Delta\nu_c = \Delta\nu_{FSR}$ and $F_c = 1$, i.e., two adjacent Lorentzian lines (dashed colored lines, only 5 lines are shown for clarity) cross at half maximum (solid black line) and the Taylor criterion for spectrally resolving two peaks in the resulting Airy distribution (solid purple line) is reached.

Optics EXPRESS

4.2 Scanning the Fabry-Pérot resonator: Airy linewidth and finesse

A different situation occurs when the Fabry-Pérot resonator is used as a scanning interferometer, i.e., at varying resonator length (or angle of incidence), to spectroscopically distinguish spectral lines at different frequencies within one free spectral range. In this case several Airy distributions, each one created by an individual spectral line, must be resolved. Therefore, now the Airy distribution becomes the underlying fundamental function and the measurement delivers a sum of Airy distributions. The parameters that properly quantify this situation are the Airy linewidth $\Delta\nu_{Airy}$ and the Airy finesse F_{Airy}.

On either side of the peak of Eq. (35) located at ν_q, the transmitted intensity decreases to $A'_{trans}(\nu_q)/2$ when the phase shift ϕ changes by the amount $\Delta\phi$ and, accordingly, $\sin^2(\phi)$ changes from 0, such that in the denominator of A_{circ} of Eq. (19)

$$4\sqrt{R_1R_2}\sin^2(\Delta\phi) = \left(1-\sqrt{R_1R_2}\right)^2 \;\Rightarrow\; \Delta\phi = \arcsin\left(\frac{1-\sqrt{R_1R_2}}{2\sqrt[4]{R_1R_2}}\right). \tag{47}$$

Exploiting Eqs. (10) and (11) to calculate $\phi = \pi\nu/\Delta\nu_{FSR}$, resulting in $\Delta\phi = \pi(\Delta\nu_{Airy}/2)/\Delta\nu_{FSR}$, then provides the FWHM linewidth $\Delta\nu_{Airy}$ of the Airy distribution [5],

$$\Delta\nu_{Airy} = \Delta\nu_{FSR}\frac{2}{\pi}\arcsin\left(\frac{1-\sqrt{R_1R_2}}{2\sqrt[4]{R_1R_2}}\right). \tag{48}$$

The Airy linewidth $\Delta\nu_{Airy}$ is displayed as the green curve in Figs. 6(a) and 6(c) in direct comparison with the Lorentzian linewidth $\Delta\nu_c$. The ratio between $\Delta\nu_{Airy}$ of Eq. (48) and $\Delta\nu_c$ of Eq. (16) is displayed in Fig. 6(e).

The concept of defining the linewidth of the Airy peaks as FWHM breaks down at $\Delta\nu_{Airy} = \Delta\nu_{FSR}$ (solid red line in Fig. 4), because at this point the Airy linewidth instantaneously jumps to an infinite value. For lower reflectivity values R_1R_2, the FWHM linewidth of the Airy peaks is undefined and other definitions or concepts would have to be utilized to describe the situation. The limiting case occurs at

$$\Delta\nu_{Airy} = \Delta\nu_{FSR} \;\Rightarrow\; \frac{1-\sqrt{R_1R_2}}{2\sqrt[4]{R_1R_2}} = 1 \;\Rightarrow\; R_1R_2 = 17-12\sqrt{2} \approx 0.02944. \tag{49}$$

For equal mirror reflectivities, this point is reached when $R_1 = R_2 \approx 17.2\%$ (solid red line in Fig. 4). A number of fiber and channel waveguide lasers that produce very high gain due to their strong pump confinement are operated in resonators that rely solely on the Fresnel reflection on both ends of the resonator, which is typically below this value. I.e., we are operating numerous laser resonators whose passive Airy linewidth $\Delta\nu_{Airy}$ is undefined. Nevertheless, no problem arises from it, because the appropriate parameters in the situation of the lasing Fabry-Pérot resonator are its Lorentzian linewidth $\Delta\nu_c$ and finesse F_c.

Definitions can never be right or wrong. They can only be more or less meaningful and, in the worst case, contradict with another more or less meaningful definition. The finesse of the Airy distribution of a Fabry-Pérot resonator, which is displayed as the green curve in Figs. 6(b) and 6(d) in direct comparison with the Lorentzian finesse F_c, is properly defined as

$$F_{Airy} \overset{!}{:=} \frac{\Delta\nu_{FSR}}{\Delta\nu_{Airy}} = \frac{\pi}{2}\left[\arcsin\left(\frac{1-\sqrt{R_1R_2}}{2\sqrt[4]{R_1R_2}}\right)\right]^{-1}. \tag{50}$$

When scanning the length of the Fabry-Pérot resonator (or alternatively the angle of incident light), the Airy finesse lucidly quantifies the maximum number of Airy distributions created by light at individual frequencies ν_m within the free spectral range of the Fabry-Pérot

Optics EXPRESS

resonator, whose adjacent peaks can be unambiguously distinguished spectroscopically, i.e., they do not overlap at their FWHM (Fig. 8). Consequently, this definition of the Airy finesse is consistent with the Taylor criterion of the resolution of a spectrometer and is, therefore, denoted by an exclamation mark in Eq. (50). Since the concept of the FWHM linewidth breaks down at $\Delta\nu_{Airy} = \Delta\nu_{FSR}$, consequently the Airy finesse is defined only until $F_{Airy} = 1$, see Fig. 6(d), because the arcsin function in Eq. (50) cannot produce values above $\pi/2$.

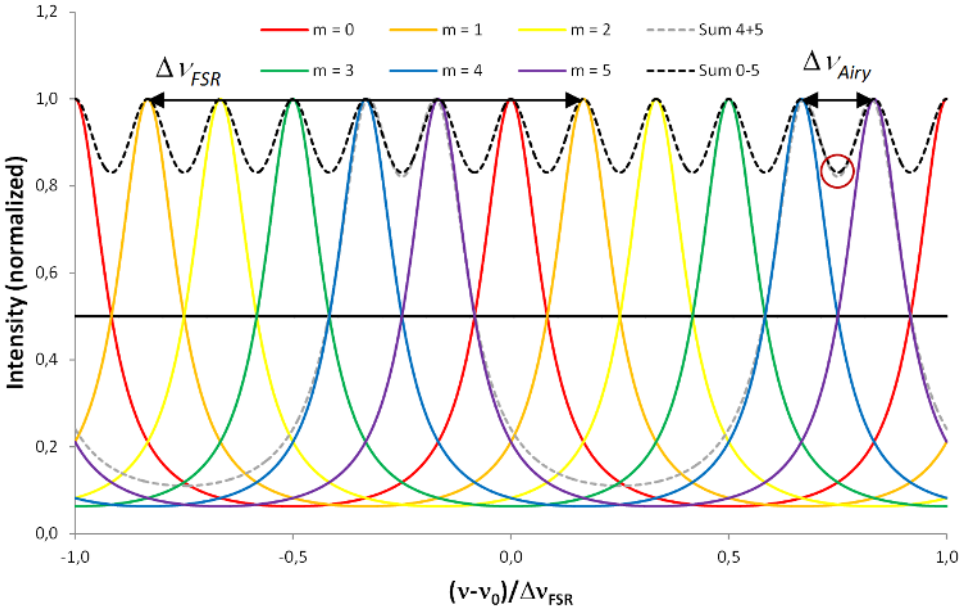

Fig. 8. Illustration of the physical meaning of the Airy finesse F_{Airy} of a Fabry-Pérot resonator. When scanning the Fabry-Pérot length (or alternatively the angle of incident light), Airy distributions (solid lines) are created by signals at individual frequencies. If the signals occur at frequencies $\nu_m = \nu_q + m\Delta\nu_{Airy}$, where m is an integer starting at q, the Airy distributions at adjacent frequencies are separated from each other by the linewidth $\Delta\nu_{Airy}$, thereby fulfilling the Taylor criterion for the spectroscopic resolution of two adjacent peaks. The maximum number of signals that can be resolved is F_{Airy}. Since in this specific example the reflectivities $R_1 = R_2 = 0.59928$ have been chosen such that $F_{Airy} = 6$ is an integer, the signal for $m = F_{Airy}$ at the frequency $\nu_q + F_{Airy}\Delta\nu_{Airy} = \nu_q + \Delta\nu_{FSR}$ coincides with the signal for $m = q$ at ν_q. In this example, a maximum of $F_{Airy} = 6$ peaks can be resolved when applying the Taylor criterion. However, the sum of two adjacent "resolvable" peaks (dashed gray line) exhibits a deeper dip between the adjacent peaks to be resolved, i.e., a better resolution, than the sum of all "resolvable" peaks (dashed black line), see the difference highlighted in the red circle.

Generally, one can argue that the Taylor criterion leaves some ambiguity to the definition of the limit of spectral resolution, because it does not state whether it requires the absence or allows for the presence of additional resolvable spectral lines. In the example of Fig. 8, the sum of two adjacent "resolvable" Airy distributions (dashed gray line) is better resolvable than the sum of all "resolvable" Airy distributions (dashed black line), because in the latter case additional Airy distributions contribute, see the dashed lines within the red circle in Fig. 8. If either of the two options defines the limit of spectral resolution, the other cannot.

4.3 Questionable approximations and definitions

Often the unnecessary approximation $\sin(\phi) \approx \phi$ is made when deriving from A'_{trans} of Eq. (31) or Eq. (38) the Airy linewidth [2,8]. In contrast to the exact Eqs. (47) and (48), it leads to

$$4\sqrt{R_1R_2}\,(\Delta\phi)^2 \approx \left(1-\sqrt{R_1R_2}\right)^2 \;\Rightarrow\; \Delta\nu_{Airy} \approx \Delta\nu_{FSR}\frac{2}{\pi}\Delta\phi = \Delta\nu_{FSR}\frac{1}{\pi}\frac{1-\sqrt{R_1R_2}}{\sqrt[4]{R_1R_2}}. \quad (51)$$

Optics EXPRESS

This approximation of the Airy linewidth, displayed as the red curve in Figs. 6(a) and 6(c), deviates from the correct curve at low reflectivities and incorrectly does not break down when $\Delta\nu_{Airy} > \Delta\nu_{FSR}$. This approximation is then typically also inserted into Eq. (50) to calculate the Airy finesse [8], resulting in

$$F_{Airy} \overset{!}{:=} \frac{\Delta\nu_{FSR}}{\Delta\nu_{Airy}} \approx \pi \frac{\sqrt[4]{R_1 R_2}}{1-\sqrt{R_1 R_2}}. \tag{52}$$

Vaughan [2] and Siegman [6] even defined the Airy finesse by its approximation of Eq. (52),

$$\widehat{F}_{Airy} \overset{?}{:=} \pi \frac{\sqrt[4]{R_1 R_2}}{1-\sqrt{R_1 R_2}} \approx \frac{\Delta\nu_{FSR}}{\Delta\nu_{Airy}}, \tag{53}$$

thereby depriving this parameter of its lucid meaning. Since the definition of Eq. (53) does not comply with the Taylor criterion, it is denoted by a question mark. Saleh and Teich [12,11] also proposed Eq. (53) for the Airy finesse, but from their derivation it remains unclear whether they consider it as a definition or as an approximation of Eq. (50).

Whereas the definitions of Airy linewidth and finesse break down at $\Delta\nu_{Airy} = \Delta\nu_{FSR}$ and $F_{Airy} = 1$, the Lorentzian linewidth $\Delta\nu_c$ and finesse F_c do not break down at a critical value. Moreover, the latter reach their Taylor limit at higher losses than the former. Therefore, useful and well defined information can be extracted from non-scanning Fabry-Pérot measurements beyond the limit of the Airy linewidth and finesse (which are irrelevant quantities for non-scanning measurements).

5. Response to frequency-dependent reflectivity

In the previous Sections we described a Fabry-Pérot resonator whose mirror reflectivities are independent of frequency. We showed that the Airy distribution is nothing else but the sum of its underlying mode profiles. Now we consider the mirror reflectivities as general functions of frequency, $R_i(\nu)$, such that the photon-decay time $\tau_c(\nu)$ of Eq. (3) becomes a function of frequency. As a result, the spectral line shapes $\tilde{\gamma}_q(\nu)$ of Eq. (15), the mode profiles $\gamma_{q,emit}(\nu)$ of Eq. (41) and all other mode profiles, as well as the Airy distribution $A_{emit}(\nu)$ of Eq. (42) and all other Airy distributions, are spectrally modified. In Eqs. (16) and (17), $\Delta\nu_c$ turns into a local function of frequency, thereby losing its meaning as the FWHM linewidth. Nevertheless, all Airy distributions fundamentally remain the sums of their corresponding mode profiles. Consequently, even for frequency-dependent reflectivities $R_i(\nu)$ we can calculate the spectral line shape $\tilde{\gamma}_q(\nu)$ and mode profile $\gamma_{q,emit}(\nu)$ of each mode directly from Eqs. (15) and (41), respectively, and obtain all other mode profiles via the simple scaling factors of Eq. (44). These spectral line shapes and mode profiles are the most general expressions for the longitudinal modes of a Fabry-Pérot resonator with frequency-dependent reflectivities.

In order to illustrate the deformation of the mode profiles and their resulting Airy distributions in a resonator with frequency-dependent reflectivities, we consider two different resonators. Both have air ($n_r = 1$) as their internal medium and identical multilayer mirrors with the reflectivity curve shown in both, Figs. 9(a) and 9(b), which is symmetric around its maximum value of 98% at 300 THz (vertical black dashed lines in Fig. 9). These resonators are distinguished only by their lengths of $\ell_1 = 999.808$ µm (left-hand side in Fig. 9) and $\ell_2 = 999.924$ µm (right-hand side in Fig. 9). Their resonance frequencies (vertical dashed lines) with mode indexes $q = 2000$ (red lines), $q = 2001$ (green lines), and $q = 2002$ (blue lines) occur at $\nu_q = 299.85$ THz, 300.00 THz, and 300.15 THz (left-hand side of Fig. 9) and $\nu_q = 299.815$ THz, 299.965 THz, and 300.115 THz (right-hand side of Fig. 9). Consequently, the nearest resonance frequency with mode index $q = 2001$ coincides with the reflectivity maximum at 300 THz, leading to a symmetric situation (left-hand side), or is spectrally offset

Optics EXPRESS

by 35 GHz, leading to an asymmetric situation (right-hand side). In order to account only for the effects of reflectivity, we neglect the penetration depth of the light inside the mirrors, which can, in principle, also be frequency dependent.

In Figs. 9(c) and 9(d), the mode profiles $\gamma_{q,emit}$ of the three nearest modes with mode indexes q = 2000, q = 2001, and q = 2002 (red, green, and blue solid lines), the numerical summation of 6 × 10^6 mode profiles, which were summed at various frequencies (magenta dots), and the Airy distribution A_{emit} (black solid line) are displayed. In both situations, the sum of mode profiles and the Airy distribution show excellent agreement (and would show perfect agreement if it were possible to extend the summation over the infinite sum of mode profiles). In the symmetric situation of Fig. 9(c), the main peak of the central mode profile (green solid line) as well as the Airy distribution (black solid line) reach a peak value of ~99, but are only shown until the value of 4 to better resolve the details of the mode profiles. In the asymmetric situation of Fig. 9(d), the mode profile of the nearest mode with q = 2001 (green solid line) and the Airy distribution (black solid line) become strongly asymmetric. The main peak of the nearest mode profile as well as the Airy distribution lies between the resonance frequency (green dashed line) and the reflectivity maximum (black dashed line). The main peak of the mode profile has a FWHM linewidth of 7.2 GHz that is significantly narrower than the FWHM linewidth of 118.7 GHz that would occur if the photon-decay time τ_c were constant with frequency and determined by the reflectivity value of 8.3% at the mode's resonance frequency of ν_{2001} = 299.965 THz. The spectral dependence of the mode profiles $\gamma_{q,emit}$ is determined by the internal resonance enhancement factor A_{circ} and the simple scaling factor $1-R_1(\nu)R_2(\nu)$ of Eqs. (28) or (44), which both depend on frequency. In particular, the internal resonant enhancement factor A_{circ} depends on frequency through the phase $\phi(\nu)$ and through the reflectivity curves $R_1(\nu)$ and $R_2(\nu)$ of the two resonator mirrors. A_{circ} (black solid line) is shown in Figs. 9(e) and 9(f). The peak value (not displayed in the figures) is 2500 in the symmetric situation and 7.56 in the asymmetric situation. Also shown is the Airy distribution A_{trans} (magenta solid line), whose peak value reaches 50 and 2.2 in the symmetric and asymmetric situation, respectively. The spectral contents of A_{emit}, A_{circ}, and A_{trans} and the frequencies of their main peaks differ from each other, because the scaling factors between these Airy distributions are frequency dependent. Besides A_{emit}, the distributions A_{circ} and A_{trans} are only two of the other Airy distributions related to the launched intensity I_{laun}. We leave it to the reader to calculate $A_{b\text{-}circ}$ and A_{back} and the mode profiles of all these Airy distributions and verify that, in all cases, their sums generate the corresponding Airy distributions.

Among the Airy distributions related to the incident intensity I_{inc}, the most utilized one, A'_{trans} (black solid line), is shown in Figs. 9(g) and 9(h), together with the three nearest mode profiles $\gamma'_{q,trans}$ (red, green, and blue solid lines) and the sum of 6 × 10^6 mode profiles (magenta dots). At the resonance frequencies A'_{trans} becomes unity. In addition, whenever the reflectivity curve in Figs. 9(a) and 9(b) approaches zero, A'_{trans} approaches unity, but obviously these peaks do not represent resonances. In Fig. 9(g), the resonance with mode index q = 2001 is located in the center of the reflection band and identified as a resonance line, whereas in Fig. 9(h) it almost coincides with a frequency of zero reflection and, thus, does not appear as a separate peak. Like for A'_{trans}, those non-resonant peaks occur for all other Airy distributions. The Airy distributions A'_{circ} (black solid line) and A'_{emit} (magenta solid line) are displayed in Figs. 9(i) and 9(j). In the symmetric situation, A'_{circ} extends to 50 and A'_{emit} to 1.98, whereas in the asymmetric situation A'_{circ} extends to 2.2 and A'_{emit} to 1.42.

Optics EXPRESS

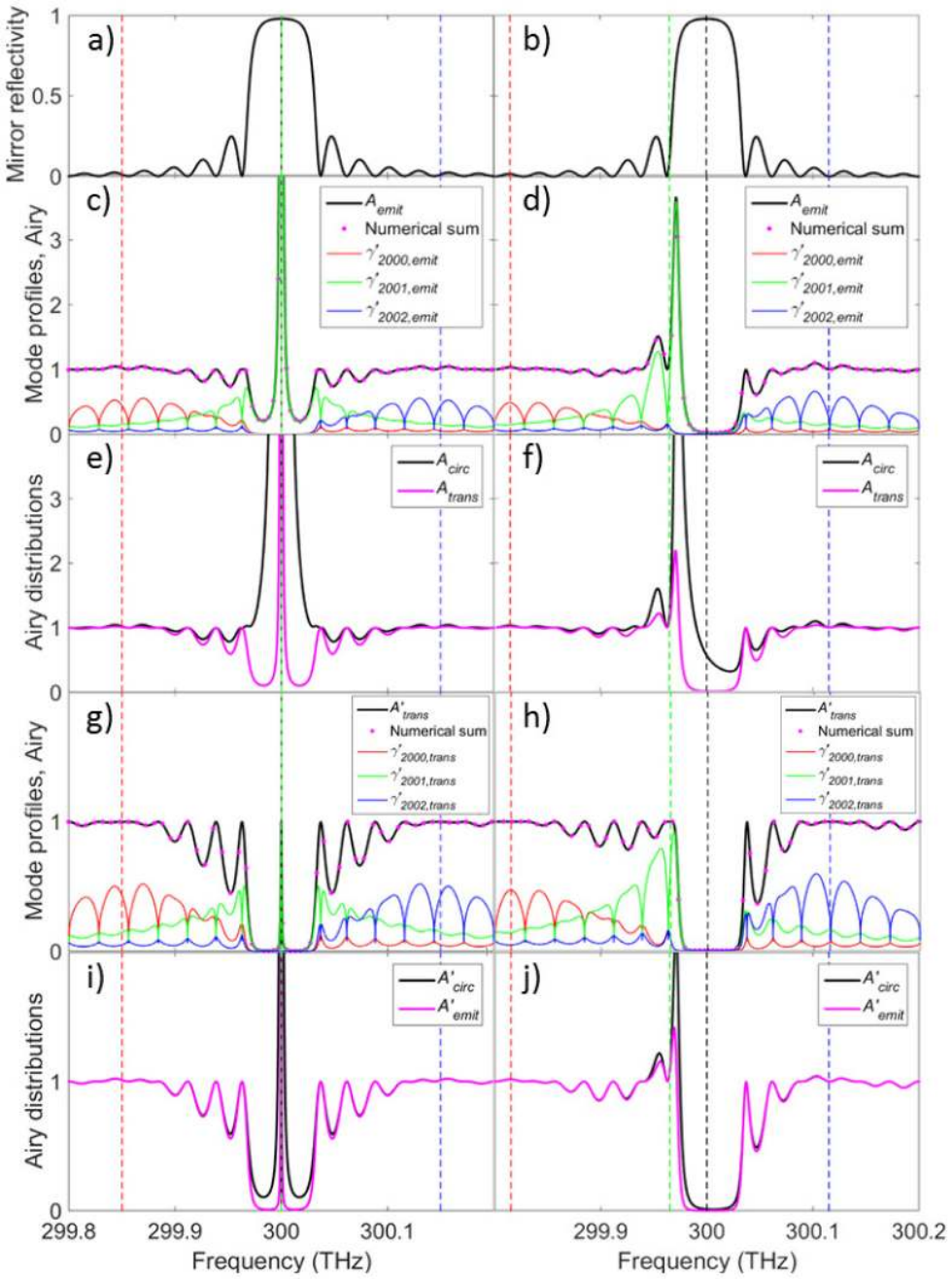

Fig. 9. Spectral investigation of resonators with their nearest resonance frequency (dashed green vertical line) coinciding with (left), or offset by 35 GHz (right) from the reflectivity maximum (dashed black vertical line). Dashed red and blue vertical lines: next resonance frequencies. (a), (b) Mirror reflectivity of the investigated resonators. (c), (d) Airy distributions A_{emit} calculated analytically (solid black line) and numerically as the sum of mode profiles (magenta dots). Red, green, and blue solid lines: the three nearest resonator modes $\gamma_{q,emit}$. (e), (f) Airy distributions A_{circ} and A_{trans}. (g), (h) Airy distributions A_{emit}, calculated analytically (solid black line) and numerically as the sum of mode profiles (magenta dots). Red, green, and blue solid lines: mode profiles $\gamma'_{q,trans}$ of the three nearest resonator modes. (i), (j) Airy distributions A'_{circ} and A'_{emit}, calculated analytically.

Optics EXPRESS

In all cases, the mode profiles are spectrally modified by the reflectivity curve. They obtain large values around their resonance frequencies ν_q, but their spectral center of mass usually does not coincide with their resonance frequency.

One can numerically sum a large number $M = 2m + 1$, for q ranging from $-m$ to m, of mode profiles and reproduce the corresponding Airy distribution. Examples are shown in Figs. 9(c) and 9(d) for the mode profiles $\gamma_{q,emit}$ and the Airy distribution A_{emit} and in Figs. 9(g) and 9(h) for the mode profiles $\gamma'_{q,trans}$ and the Airy distribution A'_{trans}. The error ϵ decreases towards zero as M increases to infinity. Empirically we find that for sufficiently large values of M, such that the product $m \times \Delta\nu_{FSR}$ is larger than the frequency at which the error is evaluated, the error ϵ follows a monomial function $\epsilon(M) = \varepsilon M^{-1}$. When the contributions of those modes resonating at frequencies that are very distant from the frequency under investigation become too small for the numerical addition to work properly, eventually one runs into numerical errors. These can be reduced by using variable precision arithmetic or by special summation algorithms such the Kahan summation [21].

Now we assume, firstly, that the mirror reflectivities change slowly with frequency, such that they are almost constant over each free spectral range, $R_i(\nu_q - \Delta\nu_{FSR}/2) \approx R_i(\nu_q) \approx R_i(\nu_q + \Delta\nu_{FSR}/2)$. Secondly, we assume that the spectral line shape of each mode is mostly confined to a free spectral range, i.e., its linewidth is $\Delta\nu_q < \Delta\nu_{FSR}$. These two assumptions would provide a justification to approximate the mode profiles by Lorentzian-shaped mode profiles. However, these Lorentzian-shaped mode profiles would be different from each other, $\Delta\nu_{q1} \neq \Delta\nu_{q2}$, because $R_i(\nu_{q1}) \neq R_i(\nu_{q2})$. When summing these Lorentzian-shaped mode profiles, the error we would make in the evaluation of the Fabry-Pérot transmission would never decrease to zero with increasing number of summation terms, but would converge to a constant value. Furthermore, for specific frequencies the error may also assume negative values which may, in specific situations, lead to the unrealistic outcome of the relative transmission A'_{trans} exceeding unity. We verified numerically that the proposed approximation would lead to errors below 5×10^{-6} only for slowly varying reflectivities (with respect to the free spectral range) in the range of 0.02% variation per THz, and for large reflectivity values near 80% reflectivity, such that the spectral mode shape is mostly contained within a free spectral range. For reflectivity variations of ~0.085% (or 0.02%) per THz and minimum reflectivities reaching 17.2%, the error stays below 1×10^{-4} (or 1×10^{-5}).

6. Conclusions

As we have demonstrated in this paper, the understanding that the Airy distribution describing the spectral transmission of a Fabry-Pérot resonator physically originates in the sum of mode profiles of the longitudinal resonator modes has fundamental consequences. The resonator losses are related to the linewidth of the Lorentzian lines rather than the linewidth of the Airy distribution. Hence, a new parameter, the Lorentzian finesse, becomes important. Whereas the concept of Airy linewidth and finesse breaks down at low reflectivity, the Lorentzian linewidth and finesse are still well defined, thus allowing for a correct characterization of the Fabry-Pérot resonator. Once the internal resonance enhancement, equaling the generic Airy distribution that characterizes the light intensity that is forward circulating inside the resonator, is known, all other Airy distributions of back-circulating, transmitted, back-transmitted, and total emitted light intensity can be derived by simple scaling factors. Furthermore, in the case of frequency-dependent mirror reflectivities, the deformed spectral line shapes and mode profiles of the underlying modes can be derived from the same simple equations. Also in this generalized situation, each sum of mode profiles generates the corresponding Airy distribution.

Especially the characterization of Fabry-Pérot resonators with low reflectivity, high loss, or strongly frequency-dependent mirror reflectivities, such as distributed-Bragg-reflector and distributed-feedback resonators as well as any type of micro-resonator, which nowadays are routinely applied in high-gain lasers and nano-optics, respectively, will profit from the fundamental insight provided in this paper.

Optics EXPRESS

Appendix

A. Derivation of Airy distribution of reflected intensity

In the situation of Fig. 1, the back-transmitted electric field is

$$E_{back} = it_1 r_2 E_{circ} e^{-i2\phi} \;\Rightarrow\; \frac{E_{back}}{E_{inc}} = \frac{-t_1^2 r_2 e^{-i2\phi}}{1 - r_1 r_2 e^{-i2\phi}}. \tag{54}$$

Including the initially back-reflected electric field, $E_{refl,1} = r_1 E_{inc}$, the total electric field propagating backward from mirror 1 is

$$\frac{E_{refl}}{E_{inc}} = \frac{E_{refl,1} + E_{back}}{E_{inc}} = r_1 + \frac{-t_1^2 r_2 e^{-i2\phi}}{1 - r_1 r_2 e^{-i2\phi}} = \frac{r_1 - r_2 e^{-i2\phi}}{1 - r_1 r_2 e^{-i2\phi}}. \tag{55}$$

Exploiting the identities

$$\left|e^{-i\phi}\right|^2 = \left|\cos(\phi) - i\sin(\phi)\right|^2 = \cos^2(\phi) + \sin^2(\phi) = 1, \quad \cos(2\phi) = 1 - 2\sin^2(\phi) \tag{56}$$

yields

$$\begin{aligned} \left|1 - r_1 r_2 e^{-i2\phi}\right|^2 &= \left|1 - r_1 r_2 \cos(2\phi) + i r_1 r_2 \sin(2\phi)\right|^2 = \left[1 - r_1 r_2 \cos(2\phi)\right]^2 + r_1^2 r_2^2 \sin^2(2\phi) \\ &= 1 + R_1 R_2 - 2\sqrt{R_1 R_2}\cos(2\phi) = \left(1 - \sqrt{R_1 R_2}\right)^2 + 4\sqrt{R_1 R_2}\sin^2(\phi), \end{aligned} \tag{57}$$

$$\begin{aligned} \left|r_1 - r_2 e^{-i2\phi}\right|^2 &= \left|r_1 - r_2\cos(2\phi) + i r_2 \sin(2\phi)\right|^2 = \left[r_1 - r_2\cos(2\phi)\right]^2 + \left[r_2 \sin(2\phi)\right]^2 \\ &= R_1 + R_2 - 2\sqrt{R_1 R_2}\cos(2\phi) = R_1 + R_2 - 2\sqrt{R_1 R_2}\left[1 - 2\sin^2(\phi)\right]. \\ &= \left(\sqrt{R_1} - \sqrt{R_2}\right)^2 + 4\sqrt{R_1 R_2}\sin^2(\phi) \end{aligned} \tag{58}$$

The total relative intensity propagating backward from mirror 1 amounts to

$$\begin{aligned} A'_{refl} &= \frac{I_{refl}}{I_{inc}} = \frac{\left|E_{refl}\right|^2}{\left|E_{inc}\right|^2} = \frac{\left|r_1 - r_2 e^{-i2\phi}\right|^2}{\left|1 - r_1 r_2 e^{-i2\phi}\right|^2} = \frac{\left(\sqrt{R_1} - \sqrt{R_2}\right)^2 + 4\sqrt{R_1 R_2}\sin^2(\phi)}{\left(1 - \sqrt{R_1 R_2}\right)^2 + 4\sqrt{R_1 R_2}\sin^2(\phi)}, \\ \Rightarrow\; A'_{trans} + A'_{refl} &= \frac{I_{trans} + I_{refl}}{I_{inc}} = 1 \end{aligned} \tag{59}$$

as expected for a resonator that exhibits only outcoupling losses.

B. Calculation of the integral resonant enhancement

The integral of the internal resonant enhancement factor A_{circ} of Eq. (19) can be written as

$$\begin{aligned} A_{FSR} &= \frac{1}{\pi}\int_{-\pi/2}^{\pi/2} A_{circ}\, d\phi = \frac{1}{\pi}\int_{-\pi/2}^{\pi/2} \frac{1}{\left(1 - \sqrt{R_1 R_2}\right)^2 + 4\sqrt{R_1 R_2}\sin^2(\phi)}\, d\phi, \\ &= a\int_{-\pi/2}^{\pi/2} \frac{1}{b + \sin^2(\phi)}\, d\phi \end{aligned} \tag{60}$$

where a and b are given by

Optics EXPRESS

$$a = \frac{1}{4\pi\sqrt{R_1 R_2}}, \qquad b = \frac{\left(1-\sqrt{R_1 R_2}\right)^2}{4\sqrt{R_1 R_2}}, \tag{61}$$

respectively. This type of integral is solved by making the substitution $\phi = \arctan(x) \Rightarrow x = \tan(\phi)$ and expressing $\sin(\phi)$ and $d\phi$ in terms of x as follows:

$$\begin{aligned} &\sin(\phi) = \frac{\tan(\phi)}{\sqrt{1+\tan^2(\phi)}} = \frac{x}{\sqrt{1+x^2}}, \ \cos(\phi) = \frac{1}{\sqrt{1+\tan^2(\phi)}} = \frac{1}{\sqrt{1+x^2}}. \\ &\Rightarrow \ \frac{dx}{d\phi} = \frac{d\tan(\phi)}{d\phi} = \frac{1}{\cos^2(\phi)} = 1+x^2 \ \Rightarrow \ d\phi = \frac{dx}{1+x^2} \end{aligned} \tag{62}$$

The integral can be written in a simpler form as

$$\begin{aligned} A_{FSR} &= a\int_{-\pi/2}^{\pi/2} \frac{1}{b+\sin^2(\phi)}\,d\phi = a\int_{-\tan(\pi/2)}^{\tan(\pi/2)} \frac{1}{b+x^2/\left(1+x^2\right)}\frac{1}{1+x^2}\,dx \\ &= \frac{a}{(b+1)}\int_{-\tan(\pi/2)}^{\tan(\pi/2)} \frac{1}{b/(b+1)+x^2}\,dx = \frac{a/(b+1)}{\sqrt{b/(b+1)}}\left[\arctan\left(\frac{x}{\sqrt{b/(b+1)}}\right)\right]_{-\tan(\pi/2)}^{\tan(\pi/2)} \\ &= \frac{a}{(b+1)}\frac{\pi}{\sqrt{b/(b+1)}} = \frac{1}{1-R_1R_2} \end{aligned}. \tag{63}$$

C. Derivation of the sum of mode profiles

With the definitions

$$R := \sqrt{R_1 R_2} \ \Rightarrow \ \delta_{out} := -\ln(R) = -\frac{1}{2}\ln\left(R_1 R_2\right) = \frac{t_{RT}}{2\tau_c}, \tag{64}$$

where we made use of Eq. (2) and assumed a resonator that exhibits only outcoupling losses, we can write the spectral line shapes (normalized to unit integral) of Eq. (15) in terms of δ_{out}, which can be a general function of frequency, as follows

$$\begin{aligned} \tilde{\gamma}_q(\nu) &= \frac{1}{\pi}\frac{1/(4\pi\tau_c)}{1/(4\pi\tau_c)^2+\left(\nu-\nu_q\right)^2} = \frac{1}{\pi}\frac{\delta_{out}/(2\pi t_{RT})}{\left[\delta_{out}/(2\pi t_{RT})\right]^2+\left(\nu-q\Delta\nu_{FSR}\right)^2} \\ &= \frac{2\pi t_{RT}}{\delta_{out}}\frac{1}{\pi}\frac{\delta_{out}^2}{\delta_{out}^2+\left(2\pi\nu t_{RT}-2\pi t_{RT}q\Delta\nu_{FSR}\right)^2} = \frac{2t_{RT}}{\delta_{out}}\frac{\delta_{out}^2}{\delta_{out}^2+\left(2\phi-2\pi q\right)^2}. \end{aligned} \tag{65}$$

The sum of mode profiles then becomes

$$\begin{aligned} \sum_{q=-\infty}^{\infty}\gamma_{q,emit}(\nu) &= \sum_{q=-\infty}^{\infty}\frac{1}{t_{RT}}\tilde{\gamma}_q(\nu) = \frac{1}{t_{RT}}\frac{2t_{RT}}{\delta_{out}}\sum_{q=-\infty}^{+\infty}\frac{\delta_{out}^2}{\delta_{out}^2+\left(2\phi-2\pi q\right)^2} \\ &= \frac{2}{\delta_{out}}\frac{\delta_{out}}{2}\sum_{q=-\infty}^{+\infty}\left[\frac{\delta_{out}+i\left(2\phi-2\pi q\right)}{\delta_{out}^2+\left(2\phi-2\pi q\right)^2}+\frac{\delta_{out}-i\left(2\phi-2\pi q\right)}{\delta_{out}^2+\left(2\phi-2\pi q\right)^2}\right] \\ &= \frac{1}{-i2\pi}\sum_{q=-\infty}^{+\infty}\frac{1}{(\delta_{out}-i2\phi)/(-i2\pi)-q}+\frac{1}{i2\pi}\sum_{q=-\infty}^{+\infty}\frac{1}{(\delta_{out}+i2\phi)/(i2\pi)-q}. \end{aligned} \tag{66}$$

With the mathematical series [22]

Optics EXPRESS

$$\sum_{q=-\infty}^{+\infty}\frac{1}{x-q}=\pi\cot(\pi x)\ \Rightarrow\ \sum_{q=-\infty}^{\infty}\gamma_{q,emit}(\nu)=\frac{i}{2}\left[\cot\left(\frac{2\phi+i\delta_{out}}{2}\right)-\cot\left(\frac{2\phi-i\delta_{out}}{2}\right)\right]. \quad (67)$$

Expressing the cot functions as

$$\begin{aligned}&\cot(\alpha)-\cot(\beta)=\frac{\sin(\beta-\alpha)}{\sin(\alpha)\sin(\beta)}\ \Rightarrow\\&\sum_{q=-\infty}^{\infty}\gamma_{q,emit}(\nu)=\frac{i}{2}\frac{\sin(-i\delta_{out})}{\sin[\phi+i\,\delta_{out}/2]\sin[\phi-i\,\delta_{out}/2]}.\end{aligned} \quad (68)$$

With the trigonometric relations

$$\begin{aligned}&\sin(\alpha+\beta)\sin(\alpha-\beta)\\&=\left[\sin(\alpha)\cos(\beta)+\cos(\alpha)\sin(\beta)\right]\left[\sin(\alpha)\cos(\beta)-\cos(\alpha)\sin(\beta)\right]\ \Rightarrow\\&\sum_{q=-\infty}^{\infty}\gamma_{q,emit}(\nu)=\frac{i}{2}\frac{\sin(-i\delta_{out})}{\sin^2(\phi)\cos^2(i\,\delta_{out}/2)-\cos^2(\phi)\sin^2(i\,\delta_{out}/2)}\end{aligned} \quad (69)$$

and

$$\cos^2(\phi)=1-\sin^2(\phi)\ \Rightarrow\ \sum_{q=-\infty}^{\infty}\gamma_{q,emit}(\nu)=\frac{i}{2}\frac{\sin(-i\delta_{out})}{\sin^2(\phi)-\sin^2(i\,\delta_{out}/2)}. \quad (70)$$

Substituting Eq. (64) into Eq. (70) yields

$$\sum_{q=-\infty}^{\infty}\gamma_{q,emit}(\nu)=\frac{i}{2}\frac{\sin\left[i\ln(R_1R_2)/2\right]}{\sin^2(\phi)-\sin^2\left[-i\ln(R_1R_2)/4\right]}. \quad (71)$$

Finally, making use of the Euler identity

$$\begin{aligned}&\sin(x)=\frac{e^{ix}-e^{-ix}}{2i}\ \Rightarrow\\&\sum_{q=-\infty}^{\infty}\gamma_{q,emit}(\nu)=\frac{i}{2}\frac{e^{-\ln(R_1R_2)/2}-e^{\ln(R_1R_2)/2}}{2i\left\{\sin^2(\phi)-\left[e^{\ln(R_1R_2)/4}-e^{-\ln(R_1R_2)/4}\right]^2/\left[2i\right]^2\right\}}.\\&=\frac{1-R_1R_2}{\left(1-\sqrt{R_1R_2}\right)^2+4\sqrt{R_1R_2}\sin^2(\phi)}\end{aligned} \quad (72)$$

This result is used in Eq. (42).

Acknowledgments

All authors acknowledge financial support by the ERC Advanced Grant “Optical Ultra-Sensor” No. 341206 from the European Research Council.